



Article

Phase-Type Fresnel Zone Plate with Multi-Wavelength Imaging Embedded in Fluoroaluminate Glass Fabricated via Ultraviolet Femtosecond Laser Lithography

Qisong Li ^{1,2}, Xuran Dai ^{1,3} , Haosong Shi ¹, Yi Liu ^{1,4,*} and Long Zhang ^{2,4,*}

¹ Shanghai Key Lab of Modern Optical System, University of Shanghai for Science and Technology, Shanghai 200093, China; liqisong@usst.edu.cn (Q.L.); XURAN001@e.ntu.edu.sg (X.D.); shihaosong123@163.com (H.S.)

² Key Laboratory of Materials for High Power Laser, Shanghai Institute of Optics and Fine Mechanics, Chinese Academy of Sciences, Shanghai 201800, China

³ Division of Physics and Applied Physics, School of Physical and Mathematical Sciences, Nanyang Technological University, Singapore 637371, Singapore

⁴ CAS Center for Excellence in Ultra-Intense Laser Science, Shanghai 201800, China

* Correspondence: yi.liu@usst.edu.cn (Y.L.); lzhang@siom.ac.cn (L.Z.)

Abstract: Herein, we report a novel optical glass material, fluoroaluminate (AlF₃) glass, with excellent optical transmittance from ultraviolet to infrared wavelength ranges, which provides more options for application in optical devices. Based on its performance, the phase-type Fresnel zone plate (FZP) by ultraviolet femtosecond (fs) laser-inscribed lithography is achieved, which induces the refractive index change by fs-laser tailoring. The realization of ultraviolet fs-laser fabrication inside glass can benefit from the excellent optical performance of the AlF₃ glass. Compared with traditional surface-etching micro-optical elements, the phase-type FZP based on AlF₃ glass exhibits a clear and well-defined geometry and presents perfect environmental suitability without surface roughness problems. Additionally, optical focusing and multi-wavelength imaging can be easily obtained. Phase-type FZP embedded in AlF₃ glass has great potential applications in the imaging and focusing in glass-integrated photonics, especially for the ultraviolet wavelength range.

Keywords: ultraviolet femtosecond laser fabrication; inner refractive index modification; phase-type Fresnel zone plate



Citation: Li, Q.; Dai, X.; Shi, H.; Liu, Y.; Zhang, L. Phase-Type Fresnel Zone Plate with Multi-Wavelength Imaging Embedded in Fluoroaluminate Glass Fabricated via Ultraviolet Femtosecond Laser Lithography. *Micromachines* **2021**, *12*, 1362. <https://doi.org/10.3390/mi12111362>

Academic Editor: Giacomo Corrielli

Received: 18 September 2021

Accepted: 3 November 2021

Published: 4 November 2021

Publisher's Note: MDPI stays neutral with regard to jurisdictional claims in published maps and institutional affiliations.



Copyright: © 2021 by the authors. Licensee MDPI, Basel, Switzerland. This article is an open access article distributed under the terms and conditions of the Creative Commons Attribution (CC BY) license (<https://creativecommons.org/licenses/by/4.0/>).

1. Introduction

Fresnel zone plates (FZPs) are binary planar micro-optical elements consisting of a series of radially symmetric rings that can tailor the amplitude and phase of light [1,2]. This focusing mode can effectively reduce spherical aberration in comparison with refractive microlenses. In addition, because of their planar structure and low volume, FZPs can be easily incorporated into miniaturized and integrated optical systems. Owing to their attractive characteristics, FZPs have been widely used in various fields, including X-ray microscopy [3], optical trapping [4,5], pulse shaping [6], optical interconnections [7], optical imaging [8], and THz focusing [9]. To date, many methods have been developed to fabricate FZPs, such as photolithography [10], ion-beam and e-beam lithography [3,11], and femtosecond laser direct writing (FsLDW) [12–15]. However, most of these methods emphasize the use of photosensitive materials, which are generally disregarded in technical applications because of their fragile and unstable nature. The development of excellent optical dielectric materials and fabrication of FZPs based on optical materials remains one of the most significant challenges for the application of optical devices. For the fabrication of optical dielectric materials, femtosecond laser nonlinear lithography can be considered a favorable manufacturing technology to ensure precise dielectric material processing because a laser with ultrashort pulse duration can suppress the heat-affected

zone and generation of debris around the damaged crater [16,17], achieving high-precision microstructure fabrication. Usually, femtosecond laser nonlinear lithography is realized in two ways: surface ablation [18–21] and inner waveguide fabrication [22–24]. However, femtosecond laser surface ablation results in relatively large surface roughness and low optical performance. Post-processing technologies (for example, chemical etching, dry etching, and laser annealing) are imperative for surface fabrication [25–28]. The representative fabrication method of femtosecond laser lithography is proposed by Soh et al. [28]. The FZP first was fabricated on the UV photoresist by femtosecond laser direct fabrication, and then the structure was transferred onto the fused silica by the buffered oxide etch. Therefore, inner waveguide fabrication using a femtosecond laser may be a suitable candidate and requires consideration. The FZP inside Sapphire by femtosecond laser inner waveguide fabrication has also been reported [29].

However, the performance of optical dielectric materials is critical for the application of optical devices. In terms of optical dielectric materials, sapphire is the competitive candidate from the ultraviolet to the mid-infrared spectral region, but is expensive and has weak performance at high temperatures. Silicate glasses are the most common material, but they only work at visible wavelengths. Fluoride glass can be regarded as one of the most appropriate candidates for optical devices from the ultraviolet to the mid-infrared spectral region and can work under high temperatures. This can be attributed to the low intrinsic loss and distinctive glass formation system of fluoride glass. In our previous work [30,31], oxyfluorogallate glass (FGa glass) was reported to achieve excellent optical performance in the infrared wavelength range as well as structural damage characteristics resulting from fabrication using a femtosecond laser. However, considering the ultraviolet region, fluoroaluminate glass is better for fabricating ultraviolet optical devices because of its higher transmissivity compared with that of FGa glass. The microstructure fabrication on the fluoroaluminate glass induced by femtosecond laser has not been studied until now. This paper proposes a promising approach for the fabrication of fluoroaluminate glass via femtosecond-laser-inducing multiphoton absorption. This internal refractive index results change, which offers compelling advantages. The refractive index of the designated region can be tailored without any damage to the mechanical properties of the material.

We first investigated the optical transmission properties of the fluoroaluminate glass material and calculated the bandgap from the ultraviolet cutoff wavelength. The mechanism of action resulting from fabrication using a femtosecond laser was suggested based on the laser wavelength and material bandgap. Then, a phase-type FZP based on fluoroaluminate glass was fabricated via ultraviolet femtosecond laser-inscribed lithography by changing the refractive index. This type of optical device exhibits a clear and well-defined geometry in optical microscopy and is devoid of surface roughness problems, unlike traditional surface-etching micro-optical elements. Moreover, optical focusing and multi-wavelength imaging are easily achieved using the phase-type FZP. In addition, a software simulation was qualitatively performed to analyze the focusing ability of the FZP and the multi-wavelength imaging results.

2. Materials and Methods

Glass samples with a major molar composition of $35\text{AlF}_3\text{-}15\text{YF}_3\text{-}20\text{CaF}_2\text{-}10\text{MgF}_2\text{-}10\text{SrF}_2\text{-}10\text{BaF}_2$, referred to as AlF_3 glass, were prepared via conventional melting and casting at $1000\text{ }^\circ\text{C}$ for 120 min in a covered platinum crucible under a nitrogen atmosphere. After sufficient melting, the glass melt was cast by being poured into a preheated platinum mold and was annealed in a furnace near the glass transition temperature. The experimental samples were cut to a diameter of 18 mm and a thickness of 1 mm and then polished for optical property measurements. The morphology of each sample was observed using optical microscopy and field emission scanning electron microscopy (FE-SEM, ZEISS, Jena, Germany) with energy dispersive spectroscopy (EDS). The optical absorption and transmission spectra of the samples were recorded in the range of 250–3000 nm using a Perkin–Elmer Lambda 750 UV/VIS/NIR spectrophotometer.

A diagram of the FsLDW micro/nanofabrication system is shown in Figure 1. The fabrication of these samples was performed under normal atmospheric conditions using an ultrafast amplifier with direct diode-pumped technology. A central wavelength was generated at 1040 nm; two other wavelengths were generated at 520 and 343 nm, with second- and third-harmonic generation with a high repetition rate of 200 kHz. The laser wavelength λ used in the experiment was 343 nm, the pulse duration was 220 fs, and the repetition rate was 200 kHz. The objective was from Olympus with a multiple of 20 \times and an N.A. of 0.75. The output laser beam was first expanded and then entered the galvanometer system. Using the 4F lens system, the laser-focusing spot can be projected onto the objective. By designing the required structure, the data coordinates of the structure can be imported into the system-controlling software, thereby enabling 3D fabrication. In our experiments, all measurements were conducted at room temperature ($\sim 25^\circ\text{C}$).

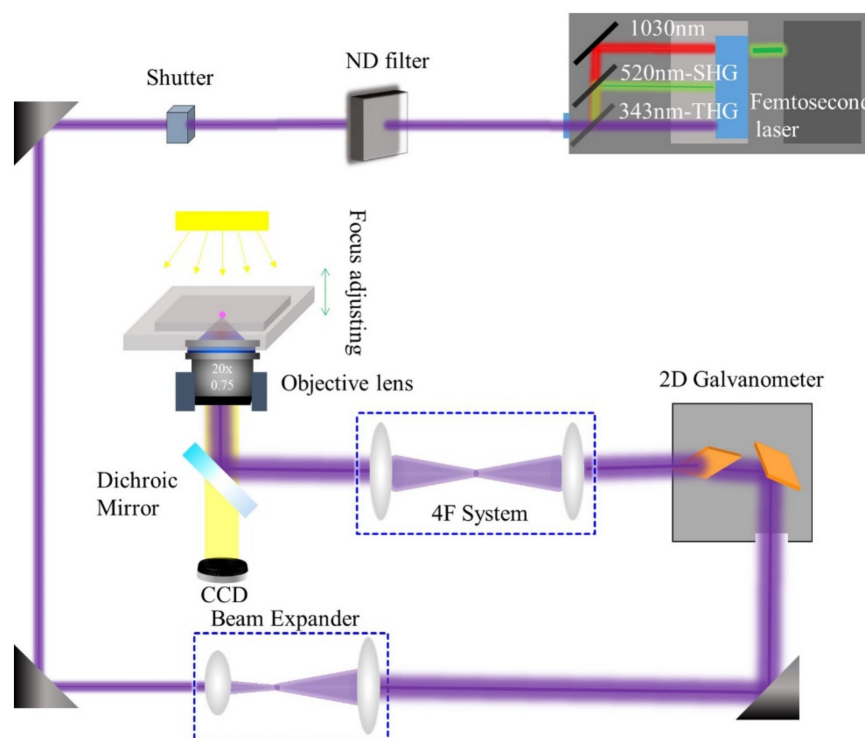


Figure 1. Schematic of experimental setup for the ultraviolet femtosecond laser fabrication.

3. Results and Discussion

Generally, a wide range of ions in glass materials play a key role in the optical performance of the glass composition, such as optical transmissivity. The optical image created by the AlF_3 glass with a ~ 5 mm thickness (Figure 2a) exhibits excellent visible transmissivity with respect to human eyes, and the letters “SIOM” can be clearly observed through the AlF_3 glass. To determine the ion composition, SEM-EDS was used to analyze the elemental details; the results are shown in Figure 2b–j. Figure 2b presents the entire EDS spectrum, in which the negative ion is the F ion, and the positive ions are Al, Y, Ca, Mg, Sr, and Ba. The map-scanning results for the corresponding ions are displayed in Figure 2d–j, and the corresponding SEM image is shown in Figure 2c. It clearly reveals the ion components of the AlF_3 glass. For optical performance, the ion excitation energy is a critical evaluation factor. Theoretically, the formula for the excitation energy can be expressed as

$$hv = E + M - \varphi \quad (1)$$

where h is Planck’s constant, v is the photon frequency, E is the electrophilic potential of the anion, M is the work done by overcoming the Coulomb action of anions and cations,

and φ is the energy gained by the anions through polarization. In this glass system, the F ion possesses a large electric potential, requiring a large amount of energy to be excited. The high valence state of the positive ions generates a large ion radius, which results in a larger excitation energy. As a result, AlF_3 glass exhibits a very short UV absorption cutoff wavelength and excellent UV optical performance.

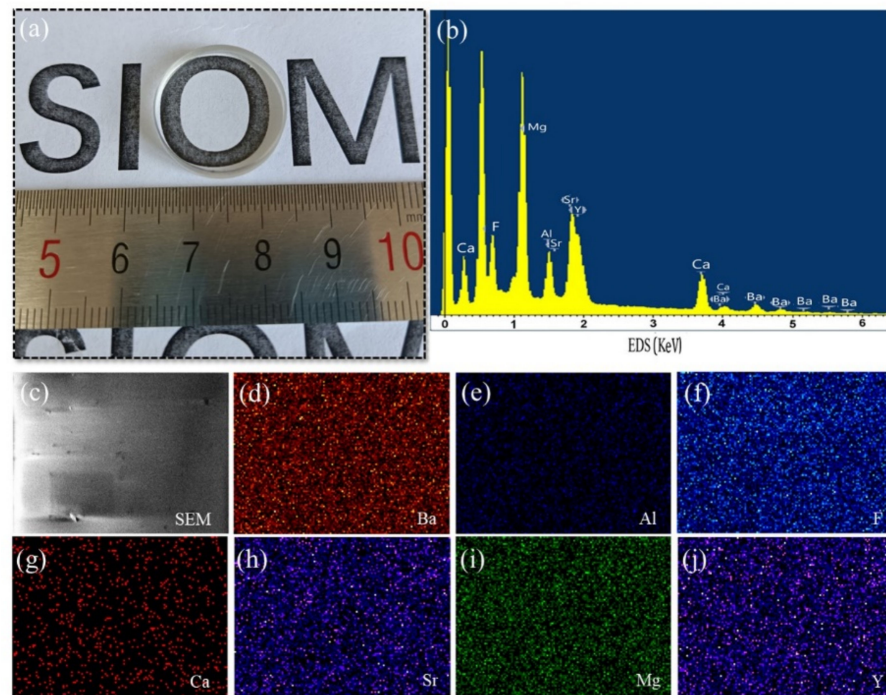


Figure 2. (a) Optical picture of the AlF_3 glass and (b–j) EDS result and the map scanning mode of AlF_3 glass for chemical elements stated.

To investigate the optical performance for potential applications in optical window materials, the UV/VIS/NIR transmission spectra for a sample thickness of ~ 1 mm were measured. The results are presented in Figure 3a. The AlF_3 glass demonstrated an excellent near-infrared and visible transmittance of $\sim 92\%$ from 400 nm to 3 μm . The transmission loss was primarily attributed to the surface Fresnel reflections and the scattering due to the sudden change in the refractive index associated with the interference between the air and the glass surface. The intrinsic absorption of the AlF_3 glass material can be ignored, and no impurities are produced during the preparation process. More importantly, the UV transmittance of AlF_3 glass can be approximately 76% at a wavelength of 250 nm, as indicated in the inset of Figure 3a. Therefore, AlF_3 glass is a suitable candidate for full-wave band optical applications, particularly in the ultraviolet wavelength range. The excellent optical transmissivity of this glass also provides the possibility of ultraviolet femtosecond laser fabrication. The absorption edge of the glass material is attributed to the bandgap (E_g), which can be calculated from the Urbach plot expressed as an $(\alpha hv)^2-hv$ diagram, using the Formula (2) [32]:

$$\begin{cases} \alpha = \frac{1}{d} \ln \frac{1}{T} \\ \alpha hv = B(hv - E_g)^{1/2} \end{cases} \quad (2)$$

where α is the linear absorption coefficient, d is the sample thickness, T is the transmissivity, and hv and B represent the photon energy and a constant, respectively. The value of the virtual bandgap E_g can be extracted from the intercept of the tangent of the Urbach plot curves, which are plotted as the calculated $(\alpha hv)^2$ versus hv , as illustrated in the inset of Figure 3b. From this curve, the bandgap energy of AlF_3 glass can be calculated as ~ 3.96 eV, corresponding to a wavelength of 313 nm ($\lambda = 1240/E_g$).

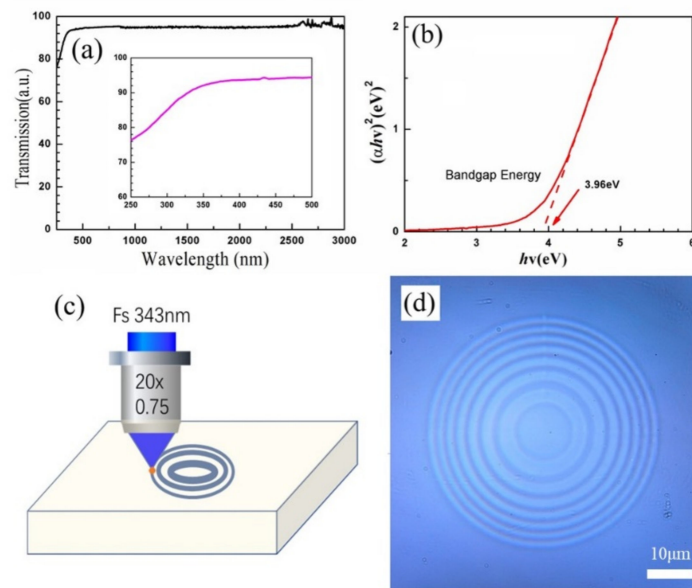


Figure 3. (a) Optical transmissivity and (b) bandgap of AlF_3 glass. The inset shows details of the ultraviolet transmissivity. (c) Fabrication diagram and (d) optical picture for the fabricated Fresnel zone plate inside the AlF_3 glass.

To leverage the excellent optical properties of AlF_3 glass, we fabricated a phase-type FZP inside the glass using ultraviolet femtosecond-laser-inscribed lithography. Considering that the laser wavelength (343 nm) is larger than the bandgap of AlF_3 glass (313 nm), two photons are required to excite an electron from the valence band to the conduction band. Thus, the nonlinear action mechanism for the femtosecond laser interaction with the AlF_3 glass can be regarded as a two-photon absorption effect, which results in a change in the refractive index. Next, we designed the FZP with the outer radius r_m of the m th zone using the following equation [25,33]:

$$r_m^2 + f^2 = (f + m\lambda/2)^2 \quad f \approx \frac{r_m^2}{m\lambda} \quad m = 1, 2, \dots, N \quad (3)$$

where f , λ , and r_m are the focus, wavelength, and outer radius of the m th zone, respectively. By controlling the focal spot inside the glass and moving along the designed path, the phase-type FZP could be fabricated by changing the refractive index via the fs-laser two-photon absorption effect. As an example, an FZP with a wavelength of 808 nm, a focus of 80 μm , and inner and outermost diameters of ~ 14 and ~ 53 μm , respectively, was adopted in our experiment. The processing laser power and scan step were optimized to be approximately 42 mW and 100 nm, respectively. A fabrication diagram of the FZP inside the glass is presented in Figure 3c. As shown in Figure 3d, the optical image provided by the phase-type FZP displays a clear profile of circular rings and a high optical contrast difference by changing the refractive index without any material damage. However, it is difficult to determine the magnitude of the change in refractive index from the femtosecond laser two-photon absorption owing to the microscale structure inside the glass. The optical performance can also be qualitatively evaluated by measuring the focusing and imaging properties.

Figure 4 shows the experimental and simulation results for the FZP in terms of the focusing performance. A semiconductor laser with a wavelength of 808 nm was used as the irradiation source. The focusing result in the transmission direction was measured at a position of ~ 81 μm , as depicted in Figure 4a. This was approximately consistent with the designed focal length. The cross-profile distribution of the optical intensity is displayed in Figure 4b. The width of the focus was approximately 2.5 μm , determined by measuring the beam size at the $1/e$ position of the full width of the beam. The ratio between the focus and

image size was approximately 0.048. Furthermore, the FZP was simulated using MATLAB to verify the focusing performance and analyze the refractive index change. In the case of the diffraction of light via an FZP, the distribution of the optical field can be calculated according to Kirchoff's diffraction formula:

$$u(\xi, \zeta) = \frac{\exp(ikz_d)}{i\lambda z_d} \int_{-\infty}^{\infty} \int_{-\infty}^{\infty} g(x, y) \exp\left\{\frac{ik}{2z_d} [((\xi - x)^2 + (\zeta - y)^2)]\right\} dx dy \quad (4)$$

$$g(x, y) = \begin{cases} \exp(i\pi\Delta n * d_p / \lambda) & \text{odd} \\ 1 & \text{even} \end{cases}$$

where $g(x, y)$ is the complex amplitude distribution of the diffraction screen, which is determined by the FZP; z_d is the distance between the FZP and the observation surface; d_p and Δn are the thickness and refractive index changes of the FZP, respectively; and (ξ, ζ) is the coordinate of the observation surface. Then, the optical field distribution can be calculated using the Fourier transform for the observation surface:

$$\begin{cases} F = \text{fftshift}(\text{fft2}(u(\xi, \zeta))) \\ I = F * \text{CONJ}(F) \end{cases} \quad (5)$$

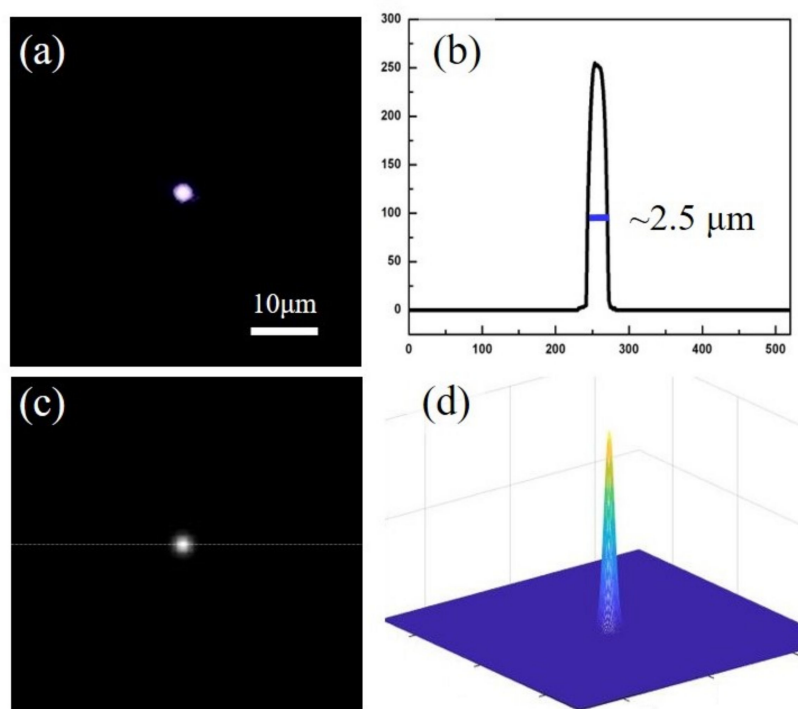


Figure 4. (a) Simulation and (b) experimental results for the focusing performance of the Fresnel zone plate under an 808 nm laser. (c,d) Corresponding sectional views of the focus intensity.

Subsequently, we simulated the focus intensity under irradiation by an 808 nm semiconductor laser, as illustrated in Figure 4a. In the simulation, we assumed that the thickness of the FZP was approximately 10 μm and that Δn was designed to be 0.01, which is the most common value of the refractive index change induced by a femtosecond laser [34]. The theoretical focusing performance of the FZP was confirmed, as shown in Figure 4c,d. We divided the observation screen for 400 px, and the focusing size was obtained at the $1/e$ position of the beam full width at the transmission position $z = 60 \mu\text{m}$. Then, we measured the ratio between the theoretical focusing size and screen size to be approximately 0.04. However, the focal position was not very accurate due to the microscale structure inside the glass, which produced an error between the measurement and the

theoretical value. Nevertheless, this simulation qualitatively demonstrated the focusing ability of the phase-type FZP. The exact measurement of the refractive index changes of the inner waveguide induced by the femtosecond laser should be performed according to the diffraction method [29].

Another important feature of the FZP is its imaging characteristics. The imaging performance of the developed FZP is presented in Figure 5a–d. Figure 5a shows an image of the letter F when white light is irradiated. It shows very clear imaging results, and the main color is blue because the CCD is more sensitive to blue light. To investigate the multi-wavelength imaging features, the lasers with different wavelengths were used as the light sources: red (633 nm), green (532 nm), and blue (405 nm). The multi-wavelength imaging results are shown in Figure 5b–d. It can be seen that this phase-type FZP has an acceptable imaging ability for red (633 nm), green (532 nm), and blue (405 nm) light. Moreover, the clear imaging positions display the increasing tendency as the wavelength increases. We then simulated the spreading light path of the FZP for different wavelengths, as shown in Figure 5e–f. The distribution of the optical field exhibits focusing paths for red (633 nm), green (532 nm), and blue (405 nm) lights. According to the light paths, a shorter wavelength of incident monochromatic light corresponds to a longer focal length, which is consistent with the equation for the FZP. Furthermore, we also measure the focal lengths of phase-type FZP for different wavelengths, which is shown in Figure 6. From the measuring results, the focus positions also display an increasing tendency as the wavelength increases and the dependence is approximately linear. Both the simulation and experimental results agree with the variation tendency observed in the imaging experiments (Figure 5b–d). Therefore, the imaging distance is directly proportional to the wavelength of the diffractive optical element, whereas it is inversely proportional to the refractive lens. The FZP devices with different materials and fabrication methods are compared in Table 1. From the comparison, it can be seen that the FZP inside AlF_3 glass by femtosecond-laser-induced refractive index change technology shows acceptable focusing and imaging properties. Due to the multi-level structure in Sapphire by the same fabrication method, the FWHM is better than that in this work. This relation can be used to eliminate chromatic aberration by combining diffractive and refractive optical elements. However, we also find that there exists some deviation for the focal lengths between the measurement in Figure 6 and the simulation in Figure 5e–f. This is because the refractive index change is not very accurate. We will try to get an accurate method to measure the refractive index change in this work and increase the focal performance in the next step.

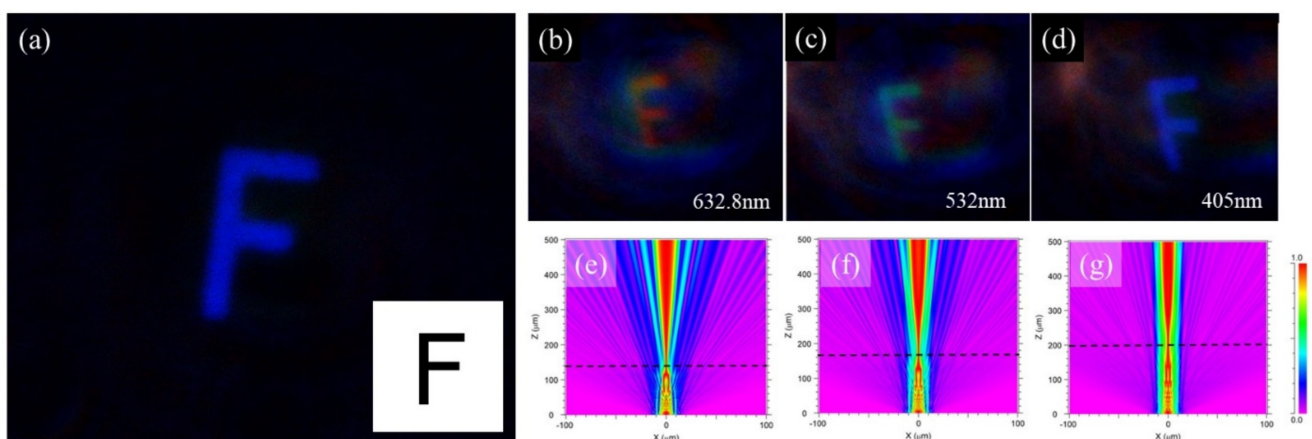


Figure 5. (a) Imaging results with a white light source. (b–d) Imaging results with red (632.8 nm), green (532 nm), and blue (405 nm) light sources. (e–g) Simulated imaging paths for the red, green, and blue lights.

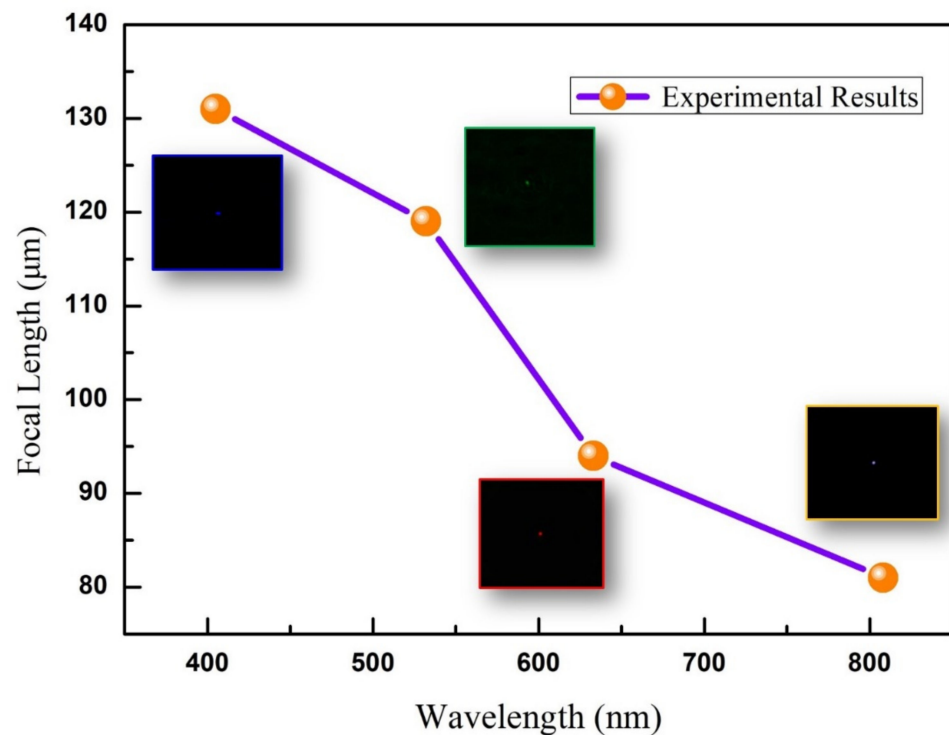


Figure 6. Experimental results for the focal length vs. different wavelengths (808 nm, 632 nm, 532 nm, and 405 nm), the insets are the pictures of the focal point.

Table 1. Comparison of the experimental results for some selected FZP devices with different materials and fabrication methods.

Fabrication Methods	Materials	FWHM	Imaging	Reference
Femtosecond laser writing and chemical etching	Sapphire	1.85 μm	Single wavelength	[25]
Laser-induced solid ablation	Metal-coated borosilicate glass	5.95 μm	Multi-wavelength	[21]
Femtosecond laser focal field engineering	Polymer	None	White light	[15]
Femtosecond laser lithography and chemical etching	Fused silica glass	2.02 μm	Single wavelength	[28]
Femtosecond-laser-induced refractive index change	Sapphire	1.75 μm with four-level FZP	Multi-wavelength	[29]
Femtosecond-laser-induced refractive index change	Fluoroaluminate glass	2.5 μm with second-level FZP	Multi-wavelength	This work

4. Conclusions

In summary, we reported a new optical material, called AlF₃ glass, which displays excellent optical performance in the ultraviolet to near-infrared wavelength range and is thus highly suitable as an optical device. We achieve the device fabrication of a phase-type FZP embedded in the AlF₃ glass using an ultraviolet femtosecond laser based on the two-photon absorption effect. The fabricated phase-type FZP exhibited a clear and well-defined geometry. Notably, it is devoid of the surface roughness problem associated with laser surface processing and presents perfect environmental suitability. More importantly, optical focusing and multi-wavelength imaging were achieved by the phase-type FZP, which was confirmed through the simulation. This novel glass and microstructures with such merits can be used in practical applications requiring exceptional ultraviolet micro-optics, such as hybrid diffractive/refractive achromatic systems.

Author Contributions: Conceptualization, Q.L.; methodology, Q.L. and L.Z.; software, X.D. and H.S.; validation, Q.L., Y.L., and L.Z.; formal analysis, Q.L. and Y.L.; investigation, Q.L., Y.L., and L.Z.; resources, Q.L. and L.Z.; data curation, Q.L., X.D., Y.L., and L.Z.; writing—original draft preparation, Q.L. and X.D.; writing—review and editing, Y.L. and L.Z.; supervision, Y.L. and L.Z.; funding acquisition, Q.L. All authors have read and agreed to the published version of the manuscript.

Funding: This work was supported by the National Science Foundation of China (No. 61905263).

Data Availability Statement: Not applicable.

Acknowledgments: The authors would like to thank Xinqiang Yuan and Xiongwei Jiang for providing the glass samples and Jianguan Hua from Jilin University for helping to test the optical performances.

Conflicts of Interest: The authors declare no conflict of interest related to this article.

References

- New, B.M. Design, Production and Performance of Circular Fresnel Zone Plates. *Appl. Opt.* **1971**, *10*, 498–503. [[CrossRef](#)]
- Hecht, E. *Optics, Fourthed*; Addison Wesley Longman Inc.: Boston, MA, USA, 1998.
- Keskinbora, K.; Grévent, C.; Bechtel, M.; Weigand, M.; Goering, E.; Nadzeyka, A.; Peto, L.; Rehbein, S.; Schneider, G.; Follath, R.; et al. Ion beam lithography for Fresnel zone plates in X-ray microscopy. *Opt. Express* **2013**, *21*, 11747–11756. [[CrossRef](#)]
- Yoon, G.; Jang, J.; Mun, J.; Nam, K.T.; Rho, J. Metasurface zone plate for light manipulation in vectorial regime. *Commun. Phys.* **2019**, *2*, 156. [[CrossRef](#)]
- Vijayakumar, A.; Bhattacharya, S. Design, fabrication, and evaluation of a multilevel spiral-phase Fresnel zone plate for optical trapping. *Appl. Opt.* **2012**, *51*, 6038–6044. [[CrossRef](#)] [[PubMed](#)]
- Cao, Q.; Jahns, J. Modified Fresnel zone plates that produce sharp Gaussian focal spots. *J. Opt. Soc. Am. A* **2013**, *20*, 1576–1581. [[CrossRef](#)] [[PubMed](#)]
- Jung, Y.J.; Park, D.; Koo, S.; Yu, S.; Park, N. Metal slit array Fresnel lens for wavelength-scale optical coupling to nanophotonic waveguides. *Opt. Express* **2009**, *17*, 18852–18857. [[CrossRef](#)] [[PubMed](#)]
- Pang, S.; Han, C.; Man Lee, L.; Yang, C. Fluorescence microscopy imaging with a Fresnel zone plate array based optofluidic microscope. *Lab Chip* **2011**, *11*, 3698–3702. [[CrossRef](#)] [[PubMed](#)]
- Yin, H.; Li, J.Q.; Liang, H.; Zhang, M.; Su, H.; Li, I.L. Full-transparent zone plates for THz focusing. *Chin. Opt. Lett.* **2018**, *16*, 082601. [[CrossRef](#)]
- Hoang Anh, N.N.; Rhee, H.G.; Ghim, Y.S. Design and lithographic fabrication of elliptical zone plate array with high fill factor. *Curr. Opt. Photon.* **2021**, *5*, 8–15.
- Fujita, T.; Nishihara, H.; Koyama, J. Blazed gratings and Fresnel lenses fabricated by electron-beam lithography. *Opt. Lett.* **1982**, *7*, 578–580. [[CrossRef](#)] [[PubMed](#)]
- Chen, Q.D.; Wu, D.; Niu, L.G.; Wang, J.; Lin, X.F.; Xia, H.; Sun, H.B. Phase lenses and mirrors created by laser micromanufacturing via two-photon photo-polymerization. *Appl. Phys. Lett.* **2007**, *91*, 171105. [[CrossRef](#)]
- Wu, D.; Niu, L.G.; Chen, Q.D.; Wang, R.; Sun, H.B. High efficiency multilevel phase-type fractal zone plates. *Opt. Lett.* **2008**, *24*, 2913–2915. [[CrossRef](#)] [[PubMed](#)]
- Srisungsitthisunti, P.; Ersoy, O.K.; Xu, X.F. Laser direct writing of volume modified Fresnel zone plates. *J. Opt. Soc. Am. B* **2007**, *24*, 2090–2096. [[CrossRef](#)]
- Yan, L.; Yang, D.; Gong, Q.H.; Li, Y. Rapid Fabrication of continuous surface Fresnel microlens array by femtosecond laser focal field engineering. *Micromachines* **2020**, *11*, 112. [[CrossRef](#)]
- Sanner, N.; Utéza, O.; Bussiere, B.; Coustillier, G.; Leray, A.; Itina, T.; Sentis, M. Measurement of femtosecond laser-induced damage and ablation thresholds in dielectrics. *Appl. Phys. A* **2009**, *94*, 889–897. [[CrossRef](#)]
- Uteza, O.; Bussiere, B.; Canova, F.; Chambaret, J.P.; Delaporte, P.; Itina, T.; Sentis, M. Laser-induced damage threshold of sapphire in nanosecond, picosecond and femtosecond regimes. *Appl. Surf. Sci.* **2007**, *254*, 799–803. [[CrossRef](#)]
- Vázquez, R.M.; Eaton, S.M.; Ramponi, R.; Cerullo, G.; Osellame, R. Fabrication of binary Fresnel lenses in PMMA by femtosecond laser surface ablation. *Opt. Express* **2011**, *19*, 11597–11604. [[CrossRef](#)]
- Lin, Z.Y.; Ji, L.F.; Hong, M.H. Enhancement of femtosecond laser-induced surface ablation via temporal overlapping double-pulse irradiation. *Photon. Res.* **2020**, *8*, 271–278. [[CrossRef](#)]
- Zhang, F.; Yang, Q.; Bian, H.; Hou, X.; Chen, F. Rapid fabrication of large-area concave microlens array on ZnSe. *Micromachines* **2021**, *12*, 458. [[CrossRef](#)]
- Rodrigues, V.R.M.; Thomas, J.; Santhosh, C.; Ramachandran, H.; Mathur, D. Microfabrication of Fresnel zone plates by laser induced solid ablation. *J. Opt.* **2016**, *18*, 075403. [[CrossRef](#)]
- Flamini, F.; Magrini, L.; Rab, A.S.; Spagnolo, N.; D’Ambrosio, V.; Mataloni, P.; Sciarrino, F.; Zandrini, T.; Crespi, A.; Ramponi, R.; et al. Thermally reconfigurable quantum photonic circuits at telecom wavelength by femtosecond laser micromachining. *Light Sci. Appl.* **2015**, *4*, e354. [[CrossRef](#)]

23. Zhang, Q.; Li, M.; Xu, J.; Lin, Z.J.; Yu, H.F.; Wang, M.; Fang, Z.W.; Cheng, Y.; Gong, Q.H.; Li, Y. Reconfigurable directional coupler in lithium niobate crystal fabricated by three-dimensional femtosecond laser focal field engineering. *Photon. Res.* **2019**, *7*, 503–507. [[CrossRef](#)]
24. Corrielli, G.; Atzeni, S.; Piacentini, S.; Pitsios, I.; Crespi, A.; Osellame, R. Symmetric polarization-insensitive directional couplers fabricated by femtosecond laser writing. *Opt. Express* **2018**, *26*, 15101–15109. [[CrossRef](#)]
25. Li, Q.K.; Yu, Y.H.; Wang, L.; Cao, X.W.; Liu, X.Q.; Sun, Y.L.; Chen, Q.D.; Duan, H.A.; Sun, H.B. Sapphire-based Fresnel zone plate fabricated by femtosecond laser direct writing and wet etching. *IEEE Photon. Technol. Lett.* **2016**, *28*, 1290–1293. [[CrossRef](#)]
26. Hopp, B.; Vass, C.; Smausz, T.; Bor, Z. Production of submicrometre fused silica gratings using laser-induced backside dry etching technique. *J. Phys. D Appl. Phys.* **2006**, *39*, 4843. [[CrossRef](#)]
27. Hua, J.G.; Ren, H.; Jia, A.; Tian, Z.N.; Wang, L.; Juodkazis, S.; Chen, Q.D.; Sun, H.B. Convex silica microlens arrays via femtosecond laser writing. *Opt. Lett.* **2020**, *45*, 636–639. [[CrossRef](#)] [[PubMed](#)]
28. Sohn, I.B.; Ahsan, M.S.; Noh, Y.C.; Choi, H.K.; Kim, J.T.; Ko, M.J. Fabrication of Fresnel zone plate lens in fused silica glass using femtosecond laser lithography technology. *Opt. Eng.* **2014**, *53*, 055107. [[CrossRef](#)]
29. Li, Q.K.; Lu, T.M.; Hua, J.G.; Yu, Y.H.; Wang, L.; Chen, Q.D.; Juodkazis, S.; Sun, H.B. Multilevel phase-type diffractive lens embedded in sapphire. *Opt. Lett.* **2017**, *42*, 3832–3835. [[CrossRef](#)] [[PubMed](#)]
30. Li, Q.S.; Yuan, X.Q.; Jiang, X.W.; Ju, Y.F.; Zhang, L. Femtosecond laser-induced damage characteristics of mid-infrared oxyfluorogallate glass. *Opt. Laser Technol.* **2019**, *109*, 659–665. [[CrossRef](#)]
31. Peng, Y.P.; Wang, C.F.; Yuan, X.Q.; Zhang, L. Er³⁺-doped oxyfluorogallate glass for 2.7 μm. *J. Lumin.* **2016**, *172*, 331–334. [[CrossRef](#)]
32. Hagfeldt, A.; Gratzel, M. Light-induced redox reactions in nanocrystalline systems. *Chem. Rev.* **1995**, *95*, 49–68. [[CrossRef](#)]
33. Zhu, B.; Liu, X.M.; Liu, H.G.; Liu, Y.A.; Yan, X.S.; Chen, Y.P.; Chen, X.F. Dual-wavelength focusing through Fresnel zone plate fabricated in lithium niobate crystal by femtosecond laser micromachining. *Phys. Status Solidi RRL* **2020**, *14*, 2000213. [[CrossRef](#)]
34. Macisa-Monteo, M.; Dias, A.; Sotillo, B.; Moreno Zarate, P.; Ariza, R.; Fernandez, P.; Solis, J. Waveguide tapers fabrication by femtosecond laser induced element redistribution in glass. *J. Light Technol.* **2020**, *38*, 6578–6583. [[CrossRef](#)]